Pramāṇa, Vol. 15, No. 2, August 1980, pp. 189–205. © Printed in India.

Lattice static properties of vacancy clusters and interstitials in hcp magnesium: Computer simulation studies

H K SAHU, S SRINIVASAN and K KRISHAN
Reactor Research Centre, Kalpakkam 603 102, India

MS received 24 April 1980; revised 21 June 1980

Abstract. Computer simulation studies have been made to investigate the static properties of mono-, di- and tri-vacancy clusters and of self-interstitials in hcp magnesium in different configurations. Three interatomic potentials have been chosen for which the results have been compared. A crystallite containing about 1500 atoms and a model with the interatomic interaction extending upto the fourth neighbour distance have been used. Relaxation field, defect relaxation and formation energies, strength dipole tensors and relative changes in volume in the above defects have been computed and our final results compared with those of earlier workers. The formation energies of the defects are highly sensitive to the choice of the potential whose detailed structure guides the nature of relaxation and the dipole tensors. Calculations have been done for octahedral, tetrahedral and dumb-bell interstitials of which the last is found to be the most stable.

Keywords. Computer simulation; point defects; lattice statics; hcp structure; di-vacancy; tri-vacancy; interstitials.

1. Introduction

There has been in recent years a growing interest in studies related to defects in hcp metals. Direct and indirect information is obtained experimentally through resistivity measurements (Lucasson 1975), diffuse x-ray scattering (Kapoor 1980, Ehrhart 1975) and study of irradiation behaviour of hcp metals (Daou *et al* 1978). In many of these cases structure-dependent effects are observed; for instance Eyre *et al* (1976) while reviewing the formation of large vacancy clusters during irradiation comments that hcp metals do not conform to the general pattern of clustering of vacancies developed for cubic metals.

Theoretical work on defect configurations in hcp metals have generally considered only the relaxation and formation energies of monovacancy and has followed three well-known approaches. The first looks at the problem of vacancy formation predominantly as one of electron redistribution and calculates the associated energy changes. The origin of this approach can be traced to the work of Fumi (1955) and has subsequently been given a rigorous basis by the Hohenberg-Kohn-Sham density-functional approach (Hohenberg and Kohn 1964; Kohn and Sham 1965) and the Harrison (1966) pseudopotential method. Chang and Falicov (1971), Ducharine and Weaver (1972) and Manninen *et al* (1975) have reported results for a vacancy in magnesium which give a reasonable value for its formation energy. The second approach follows the method due to Kanzaki (1957) and is further developed by Tewary (1973a). This utilises a two-body local potential and uses the techniques of lattice dynamics in the zero-frequency limit. In this method the defect Green's

function is calculated which is utilised to obtain the relaxation field around the defect. In earlier papers (Sahoo and Sahu 1978a) this formalism was applied to hcp metals. In particular the relaxation field and energies were calculated for a single vacancy in magnesium. Recently Tome *et al* (1979) applied this technique to a single vacancy in Mg using a different pair potential than the one used earlier by Sahoo and Sahu (1978 b, c). The results however show similar features. The third approach is the computer simulation technique which also uses a pair potential and has been successfully applied for cubic metals. Tome *et al* have used this for calculating the relaxation fields and energies for the octahedral and tetrahedral configurations of interstitials in magnesium. This technique has also been used in the present paper and detailed results are given for the mono-vacancy, three configurations each of di-vacancy and tri-vacancy and the three configurations—octahedral, tetrahedral and split interstitial (figure 1). We use various interatomic potentials for this purpose. Our main conclusions have been reported earlier (Sahu *et al* 1979). The plan of this paper is as follows. In §§ 2 and 3 respectively we give the numerical procedure and the potential used in this calculation. § 4 contains the results for the vacancy configurations while § 5 discusses the interstitial configurations and § 6 the conclusions.

2. Numerical procedure

A defect simulation program DEFSIM-I was developed and run on IBM 370/155 computer. It uses a suitable pair potential to simulate a crystallite at the centre of

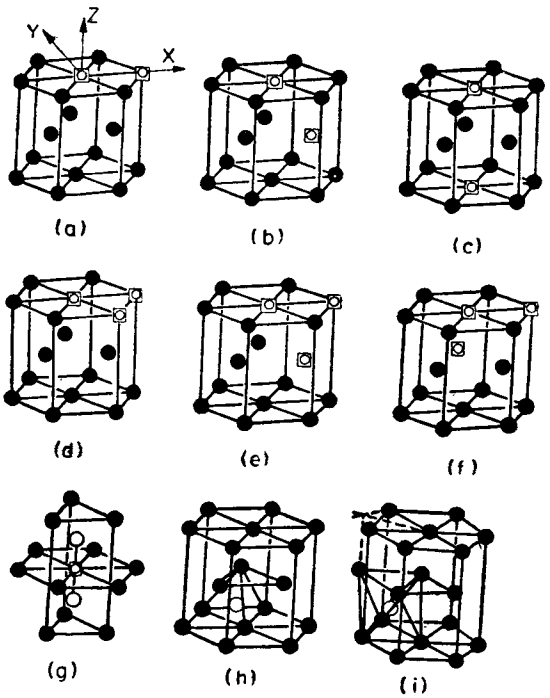

Figure 1. The three configurations each of di-vacancy and tri-vacancy and the three configurations—split, tetrahedral and octahedral interstitial.

which the defect configuration is introduced. The crystallite has two regions, the inner region I allows the atoms to freely relax to the equilibrium positions while the outer region II constrains the atoms to the perfect lattice sites. The number of atoms in region I can be increased during a run so that the relaxation field of atoms in region II is negligibly small. This enables us to ensure that the surface effects are not influencing the relaxations and also gives some saving in computational time. Initial trials with the program were performed by taking region I to contain 159, 401 and 1507 atoms corresponding roughly to 19th, 40th and 125th neighbours from the crystallite centre. The results reported in this paper are with region I containing 1507 atoms. In the calculations for vacancy and vacancy clusters even a 400-atom lattice showed sufficient convergence due to the small relaxations. Each atom interacts with the others in a region extending upto the fourth neighbour distance in the perfect lattice. The perfect crystallite contains atoms in the equilibrium positions. The crystal energy (which is minimum) is determined by summing over all the bonds of the whole crystallite. When the defect is introduced the atoms stay no more in the energy minima and so a net force develops on each atom. The configuration energy is evaluated again and the atoms are allowed to relax along the direction of atomic forces by a proportional magnitude. However, a single step of relaxation does not place the atoms in the minima of the crystal energy and hence the process is iterated until the forces vanish (i.e., the configuration energy reaches the minima again). Thus, through the iteration,

$$X_{k+1}(n) = X_k(n) - \alpha \left. \frac{\dfrac{\partial V}{\partial X(n)}}{\dfrac{\partial^2 V}{\partial X(n)^2}} \right|_{X(n)=X_k(n)}, \tag{1}$$

where $X_k(n)$ is the coordinate of the nth atom after kth iteration and V is the configuration energy. It is well-known that a direct application of the Newton-Raphson or the gradient method (where $\alpha=1$) gives very poor convergence and the relaxation tends to oscillate about the mean position. A convergence factor α was introduced in the quantum of relaxations. This simple technique damps out the oscillations and gives reasonably good convergence. The value of α, however, has to be carefully chosen by trial. Figure 2 shows typically the relaxation of an atom near a vacancy for $\alpha=1{\cdot}0$ and $\alpha=0{\cdot}75$. In the case of the interstitial configurations a much lower value of α was found necessary to get a rapid convergence.

3. Potential

The choice of a reliable two-body interatomic potential is basic to the calculation of point defect properties in both the computer simulation and in the Green's function methods. In this calculation we have used the potential given by Doneghan and Heald (1975). This potential is a fifth-order spline fitted double-well potential which as noted by them reproduces the phonon disperson data, yields the elastic force constants and the vacancy formation energy for magnesium. It is defined upto the fifth neighbour distance in four ranges by the function

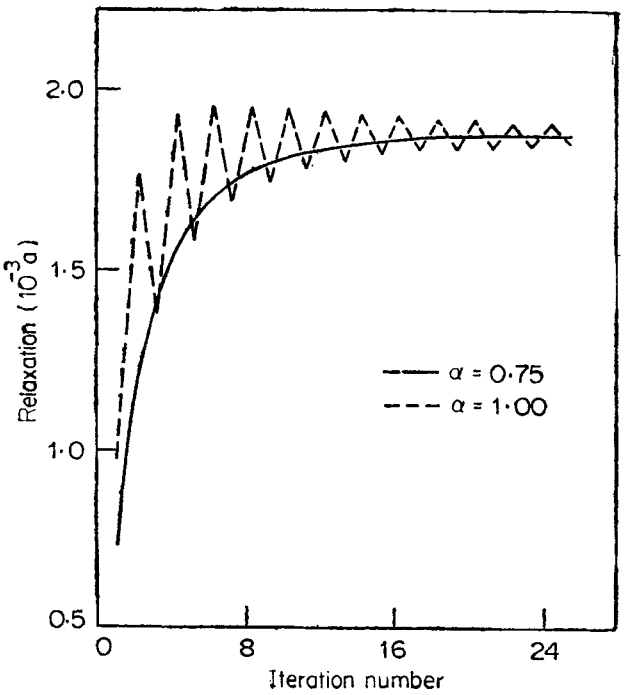

Figure 2. The influence of the convergence factor α on the relaxation behaviour of a typical atom around a single vacancy.

$$V(r) = \begin{cases} A \exp(-Br) & \text{for } r \leqslant r_1 \\ \sum_{n=0}^{5} A_{mn}[(r-r_m)/a]^n & \text{for } r_m \leqslant r \leqslant r_{m+1} \end{cases} \tag{2}$$

where m takes values 1 to 3, the basal constant a=3·21 Å, A=3829 eV, B=3·69813 Å^{-1}, r_1=0·65 a, r_2=0·996 a, r_3=1·623 a and r_4=1·729 a. The co-efficients A_{mn} are listed by Doneghan and Heald and therefore omitted here.

However, to enable one to identify features which are not potential-sensitive we have also done calculations using a potential based on the truncated Morse function

$$V(r) = -D \exp\{-\delta(r-r_0)\}\,[2 - \exp\{-\delta(r-r_0)\}], \tag{3}$$

where D, δ and r_0 are constants. Though this potential is not reliable being too steep at the short range it has been used because of its simple structure to provide a useful comparison with the results obtained using the Doneghan and Heald potential. A truncated Morse function has been used for stacking fault calculations in Mg by Schwartzkopff (1969) but the values of the parameters are not given. The values of the parameters were found by us to be D=0·1174 eV, δ=2·530148 Å^{-1} and r_0=3·213453 Å for magnesium. These values were arrived at by following the procedure discussed in detail by Doyama and Coterill (1967) for fcc metals. Applied to the case of hcp structure a four-neighbour model must give the correct bulk modulus K_0^{-1} (0·2303298 eV/Å^3), i.e.,

$$\frac{\delta D \exp(\delta r_0)}{9V} \sum_{m=1}^{4} n_m r_m [(2\delta r_m + 2) \exp\{\delta(r_0 - r_m) - (\delta r_m + 2)] \times \exp(-\delta r_m) = K_0^{-1}, \quad (4)$$

the vacancy formation energy E_{1v}^f (— 0·73 eV), i.e.,

$$\tfrac{1}{2} D \exp(\delta r_0) \sum_{m=1}^{4} n_m [\exp\{\delta(r_0 - r_m)\} - 2] \exp(-\delta r_m) = E_{1v}^f \quad (5)$$

and must satisfy the Börn stability criterion, which can be shown to be

$$\sum_{m=1}^{4} n_m Q_m [1 - \exp\{\delta(r_0 - r_m)\}] \exp(-\delta r_m) = 0. \quad (6)$$

The variables are: n_m is the number of atoms in the mth neighbour shell with radius r_m, v is the atomic volume and $Q_m = (\partial r_m / \partial a)$. A plot of the potential appears in figure 3 and the differences with the Doneghan and Heald potential are evident.

Before concluding this section it is useful to mention some of the other potentials available for magnesium. Tome *et al* (1979) used a set of cubic functions continuous in different ranges, with first and second derivatives matched at the boundary points. The short range part is similar to the Morse potential but has a steeper slope after the minimum with a small secondary minimum between the third and fourth neighbours. A comparison of our results with those reported by Tome *et al* will be given. In addition we have also used this potential to study some of the defect configurations not discussed by Tome *et al.* Rasold and Taylor (1973) and Appapillai and Heine (1972) developed pseudopotentials for magnesium. These however, have a very shallow minimum and do not reproduce the vacancy formation energy. They therefore are not particularly suitable for vacancy and vacancy cluster calculations though perhaps could be used in interstitial calculation where the short range repulsion part is more important.

4. Vacancy and vacancy clusters

4.1. *Vacancy*

Relaxation field calculations were done using the Doneghan and Heald, and the Morse potential. The relaxation field obtained till the 19th neighbours are given in figure 4 and in table 1. The magnitude of the relaxations obtained are small being of the order of $10^{-3}a$ for the first few shells surrounding the vacancy and decrease by an order of magnitude at the 19th neighbour and by another order at the 40th neighbour distance. The relative magnitudes, however, are large in the case of the Doneghan and Heald potential as far as the 10th neighbours but decrease subsequently.

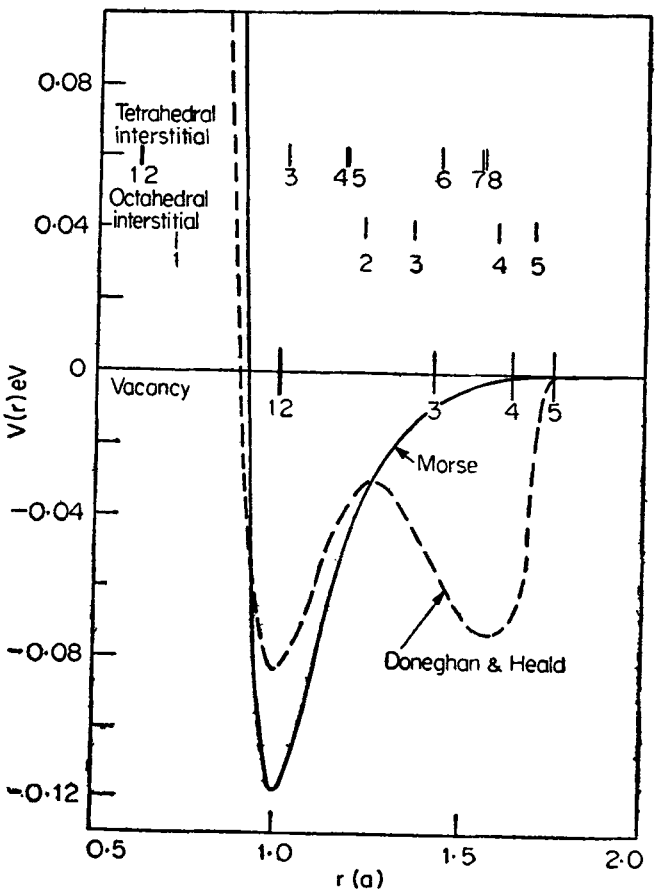

Figure 3. A plot of the Doneghan and Heald, and Morse potential function employed in the calculation.

A comparison of the relaxation fields in figure 4 obtained by the two potentials shows some interesting features. The relaxation structure of the first four shells is considerably different both in terms of relative magnitudes and signs of the relaxations. However, apart from the magnitude, the higher neighbours show some degree of correlation in terms of the relative magnitudes though there are some exceptions like the large relaxations shown in the case of the Doneghan and Heald potential. The splitting of the 6, 10, 15, 20, 28, 31, 32 and 38th shells into two groups of atoms showing different net magnitudes of the relaxations is a potential independent feature. The shell splitting can be traced to the fact that the full shell can be generated through the point group operations on two different reference atoms and the two groups of atoms in the shell do not interchange their positions under these operations. The generally large relaxations due to the negative slope at the 3rd neighbour distance in the case of the Doneghan and Heald potential is a feature also observed in the results of Tome *et al* but surprisingly they do not observe the splitting of the 6th shell. It is useful to compare our results for the single vacancy with those obtained earlier by Sahoo and Sahu (1978) using the Green's function technique. The net relaxation using the Doneghan and Heald potential for the first four shells respectively are

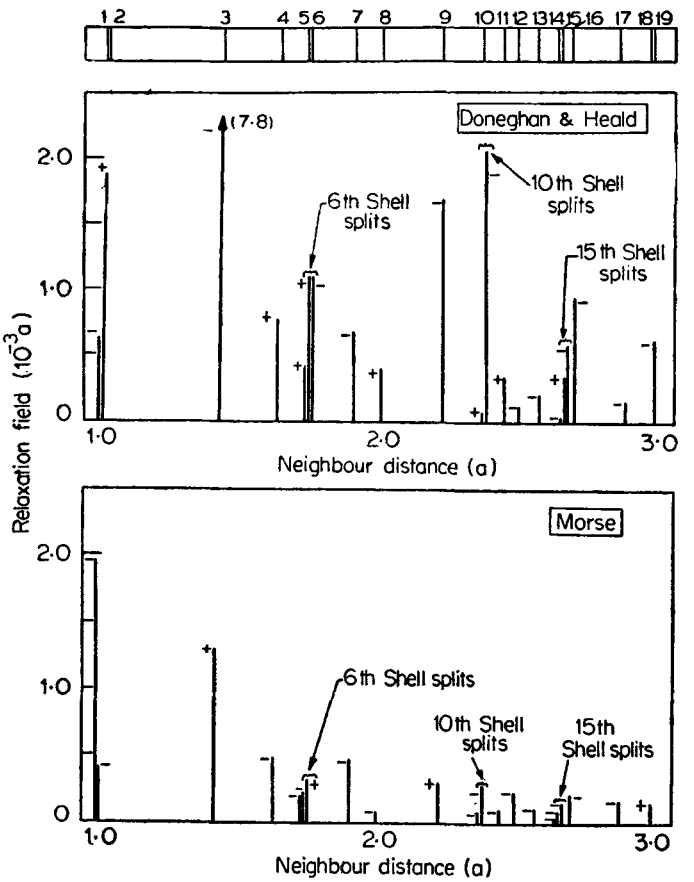

Figure 4. The relaxation field of all shells upto nineteen neighbours around a single vacancy. (+ and − signs indicate outward or inward relaxation).

Table 1. The relaxation field of all atoms upto ten neighbours around a single vacancy.

Single vacancy (0, 0, 0)

Shell Number	Neighbour position X	Y	Z	Relaxation field ($10^{-3}a$) D & H U_x	U_y	U_z	Relaxation field ($10^{-3}a$) Morse U_x	U_y	U_z
1	(−a/2	−a/2$\sqrt{3}$	c/2)	0·262	0·151	−0·563	0·740	0·427	−1·791
2	(−a/2	−$a\sqrt{3}$/2	0)	−1·873	−0·175	0·0	0·402	−0·169	0·0
3	(0	−2a/$\sqrt{3}$	c/2)	0·0	6·713	−3·988	0·0	−1·194	0·607
4	(0	0	c)	0·0	0·0	0·775	0·0	0·0	−0·508
5	(a	−2a/$\sqrt{3}$	c/2)	0·382	0·174	0·009	−0·145	0·108	−0·104
6	(3a/2	−$a\sqrt{3}$/2	0)	0·947	−0·547	0·0	−0·189	0·109	0·0
	(0	−$a\sqrt{3}$	0)	0·0	1·068	0·0	0·0	−0·315	0·0
7	(a/2	−$a\sqrt{3}$/2	c)	0·038	0·287	−0·606	−0·025	0·226	−0·413
8	(−a	−$a\sqrt{3}$	0)	−0·389	−0·076	0·0	0·061	−0·027	0·0
9	(a/2	−7a/2$\sqrt{3}$	c/2)	−0·453	1·597	−0·334	0·090	−0·289	0·036
10	(−3a/2	−$a\sqrt{3}$/2	c)	−0·094	−0·054	0·024	0·023	0·014	−0·083
	(0	−$a\sqrt{3}$	c)	0·0	1·441	−1·486	0·0	−0·182	0·203

$0{\cdot}4415\times10^{-2}a$, $0{\cdot}1666\times10^{-2}a$, $0{\cdot}7358\times10^{-2}a$, and $0{\cdot}5212\times10^{-2}a$. These are within 5% of the values obtained by us for the second and third neighbour but for the first and fourth shells our values of $0{\cdot}6380\times10^{-3}a$ and $0{\cdot}7745\times10^{-3}a$ are lower than those obtained by the Green's function method. Another feature of the relaxations which is apparent from table 1 is their non-radial character whose detailed nature is potential-dependent.

4.1*a. Relaxation energy, defect volume and strain dipole tensor.* The vacancy formation energy† $E_{1v}^f = 0{\cdot}73$ eV is correctly reproduced by both the potentials since it forms an input parameter to which the empirical potentials have been fitted. The relaxation energy for the vacancy was found to be extremely small and was $-0{\cdot}0007$ eV for the Morse potential. The Doneghan and Heald potential surprisingly does not give the estimated value of $-0{\cdot}13$ eV quoted by Doneghan and Heald (1975) but gives a small value of about $-0{\cdot}0004$ during the first few iterations which further decreased gradually with iteration number and even became positive. Careful checks were made to ensure that this behaviour was not due to the limitations of the accuracy of the numerical procedure. It was therefore not possible to evaluate the relaxation energy apart from concluding that its absolute magnitude is very small. This behaviour seems to arise from the parameters of Doneghan and Heald potential which do not exactly satisfy the Börn stability condition. However, this limitation of the potential is not too serious since the magnitude of the relaxation energy is anyway extremely small. Calculations were also made to evaluate the strength dipole tensor which in the notation of Dederichs *et al* (1978) is given by

$$P_{ij} = \sum_n R_i^{(n)} K_j^{(n)}, \tag{7}$$

where $\mathbf{R}^{(n)}$ is the distance to the nth undistorted atomic site, $\mathbf{K}^{(n)}$ is the Kanzaki force and i, j the cartesian indices. The stress dipole tensor is also related to the defect volume which is given by

$$\triangle V/V \cong \mathrm{Tr}\,\mathbf{P} \,/\, 3B_0 \tag{8}$$

where B_0 is the bulk modulus.

In the case of the vacancy the off-diagonal elements are zero, $P_{11}=P_{22}=-0{\cdot}5099$ and $P_{33}=-0{\cdot}5457$ eV for the Doneghan and Heald potential while for the Morse potential $P_{11}=P_{22}=0{\cdot}0124$ eV and $P_{33}=-0{\cdot}2360$. The ratio P_{11}/P_{33} represents the asymmetry of the interaction of the defect and is amenable to measurement through diffuse x-ray scattering. No experimental data for Mg are available for comparison. In the case of the Doneghan and Heald potential $P_{11}/P_{33}\cong0{\cdot}93$. This is in very good agreement with the results obtained by Tome *et al* who for the pseudopotential and

†The experimental E_{1v}^f is given through the empirical relation (Tewary 1973b),

$$E_{1v}^f = (MV^{2/3}/C^2)\,\theta_D^2$$

where M and V are the mass and volume of the crystal per atom, $C = 32{\cdot}8$ for all metals, and the Debye temperature θ_D is found experimentally to be 357°K. This gives $E_{1v}^f = 0{\cdot}73$ eV. The same value of E_{1v}^f is obtained also from the experimental sublimation energy data taken from the American Institute of Physics Handbook.

empirical potentials used by them obtain the value 1·02 and 0·99 respectively. The magnitudes of P_{ij} are also of the same order as obtained by them. Our results for the case of the Morse potential are substantially different and of course are not reliable, but the reason for the difference is not too difficult to see.

In table 2 the shell by shell contribution to the dipole tensor is given. The major contribution comes from the third shell and depends entirely on the slope of the potential at the third neighbour distance. The opposite slopes in the case of the Doneghan and Heald and Morse potential (and also those used by Tome *et al*) account for the difference in sign. The contribution from this shell is not very sensitive to relaxation since the slope does not change much with distance. If the contribution from this shell alone is taken into account even for the Morse potential $P_{11}/P_{33} \cong 1$. However, this is offset by the contribution from the first shell which is located near the potential minimum. The first derivative in the neighbourhood of this shell is extremely sensitive to the structure of the potential and hence to the relaxations. On the other hand the second neighbours which lie very close to the potential minimum again do not contribute much. The potential sensitivity arising from the slope of the potential near the minimum makes the ratio of the dipole tensor components to be very sensitive to the relaxation field for vacancy and vacancy clusters. This is in contrast to dipole tensor calculation for interstitials which do not show such potential sensitivity (see § 5 for example).

We conclude our discussion on the single vacancy by giving results for the relaxation volume for the vacancy obtained using equation (8). The Doneghan and Heald potential gives a value of $\triangle V/V \cong -0{\cdot}0307$ and compares well with the calculations of Sahoo and Sahu (1978c).

4.2. *Vacancy clusters*

Calculations were done for three configurations of di-vacancies and three configurations of tri-vacancies (see figure 1). Results obtained for the formation energy, binding energy, relaxation volume and stress dipole tensor for the different configurations referred to as di-vacancy (*a*), (*b*), (*c*) and tri-vacancy (*d*), (*e*), (*f*) are given in table 3 for the Doneghan and Heald potential and in table 4 for the Morse potential. The overall features are similar in many respects to the case of a single vacancy and a detailed discussion will not be given. The formation energy for the di-vacancy (*c*) which lies along the *c*-axis is the highest and binding energy least showing that this configuration would be relatively less stable than the other two configurations.

Table 2. Shellwise contribution to dipole tensor in eV for a vacancy.

Shell Number	Doneghan & Heald Potential		Morse Potential	
	$P_{11} = P_{22}$	P_{33}	$P_{11} = P_{22}$	P_{33}
1	−0·0139	−0·0552	−0·1191	−0·4701
2	0·0894	0·0	−0·0619	0·0
3	−0·5854	−0·5788	0·1933	0·1909
4	0·0	0·0883	0·0	0·0432
Total	−0·5099	−0·5457	0·0123	−0·2360

Table 3. Values of formation energy E_f, binding energy E_b, relaxation volume $\Delta V/V_{at}$ and elastic dipole tensor (all in units of eV) of di- and tri- vacancy clusters using Doneghan and Heald potential.

Defect Co-ordinates	Formation energy E_f (eV)	Binding energy E_b (eV)	Relaxation Volume $\Delta V/V_{at}$	Dipole tensor (eV) P
Single Vacancy (0, 0, 0)	0·731	—	—0·049	$\begin{pmatrix} -0.510 & 0.0 & 0.0 \\ 0.0 & -0.510 & 0.0 \\ 0.0 & 0.0 & -0.545 \end{pmatrix}$
Di-vacancy 1 (0, 0, 0) (a, 0, 0)	1·377	0·086	—0·107	$\begin{pmatrix} -1.074 & 0.0 & 0.0 \\ 0.0 & -1.074 & 0.0 \\ 0.0 & 0.0 & -1.278 \end{pmatrix}$
Di-vacancy 2 (0, 0, 0) $(a/2, -a/2\sqrt{3}, -c/2)$	1·379	0·084	—0·105	$\begin{pmatrix} -1.078 & -0.134 & 0.003 \\ -0.134 & -1.233 & -0.001 \\ 0.003 & -0.001 & -1.053 \end{pmatrix}$
Di-vacancy 3 (0, 0, 0) (0, 0, —c)	1·386	0·077	—0·101	$\begin{pmatrix} -1.029 & 0.0 & 0.0 \\ 0.0 & -1.029 & 0.0 \\ 0.0 & 0.0 & -1.174 \end{pmatrix}$
Tri-vacancy 1 (0, 0, 0) (a, 0, 0) $(a/2, a\sqrt{3}/2, 0)$	1·939	0·256	—0·182	$\begin{pmatrix} -1.799 & 0.0 & 0.0 \\ 0.0 & -1.799 & 0.0 \\ 0.0 & 0.0 & -2.235 \end{pmatrix}$
Tri-vacancy 2 (0, 0, 0) (a, 0, 0) $(a/2, -a/2\sqrt{3}, -c/2)$	1·942	0·252	—0·174	$\begin{pmatrix} -1.706 & 0.0 & 0.0 \\ 0.0 & -2.100 & 0.033 \\ 0.0 & 0.033 & -1.779 \end{pmatrix}$
Tri-vacancy 3 (0, 0, 0) (a, 0, 0) $(0, a/\sqrt{3}, -c/2)$	1·972	0·222	—0·145	$\begin{pmatrix} -1.548 & -0.159 & -0.265 \\ -0.159 & -1.502 & 0.186 \\ -0.265 & 0.186 & -1.594 \end{pmatrix}$

Between these two configurations the di-vacancy (*a*) which lies in the basal plane is slightly more stable but difference is insignificant and it is difficult to say which of the configurations di-vacancy (*a*), (*b*) would be more stable at low temperatures. Similar features are seen in the case of the tri-vacancy (*d*) which is the basal plane configuration and is most tightly bound but there is little to choose between tri-vacancy (*d*) and (*e*). The tri-vacancy (*f*) configuration is the least stable. The above features are common to both the potentials. The actual values of E^f in the case of the two potentials show a difference of about 0·03 eV and 0·1 eV between the configurations for the tri-vacancy. The di-vacancy binding is of the order of 0·1 eV and for tri-vacancies 0·3 eV. Most of the contribution comes from the bond energies. The relaxation energy E_r is nearly two orders of magnitude less. For the di-vacancy (*a*), (*b*) and (*c*) configurations E_r was —0·00154, —0·00143, —0·00137 eV respectively and for tri-vacancies (*d*), (*e*) and (*f*), —0·00205, —0·00176, —0·00232 eV respectively using the Morse potential. The Doneghan and Heald potential gave features similar to the single vacancy which was discussed earlier.

5. Interstitial configurations

5.1 *Split interstitial*

The initial configuration containing two atoms along the *c*-axis symmetrically located at a distance *c*/4 from the basal plane was allowed to relax. In the relaxed configura-

Table 4. Values of formation energy E_f, binding energy E_b, relaxaton volume $\Delta V/V_{at}$ and elastic dipole tensor (all in units of eV) of di- and tri- vacancy clusters using Morse potential.

Defect co-ordinates	Formation energy E_f (eV)	Binding energy E_b (eV)	Relaxation volume $\Delta V/V_{at}$	Dipole tensor (eV) P
Single vacancy (0, 0, 0)	0·729	—	0·0066	$\begin{pmatrix} 0·0124 & 0·0 & 0·0 \\ 0·0 & 0·0124 & 0·0 \\ 0·0 & 0·0 & -0·2360 \end{pmatrix}$
Di-vacancy 1 (0, 0, 0) (a, 0, 0)	1·341	0·117	0·0149	$\begin{pmatrix} 0·0207 & 0·0 & 0·0 \\ 0·0 & 0·0423 & 0·0 \\ 0·0 & 0·0 & -0·5423 \end{pmatrix}$
Di-vacancy 2 (0, 0, 0) ($a/2$, $-a/2\sqrt{3}$, $-c/2$)	1·342	0·117	0·0090	$\begin{pmatrix} 0·0187 & 0·0349 & -0·1161 \\ 0·0349 & 0·0589 & 0·0670 \\ -0·1161 & 0·0670 & -0·3652 \end{pmatrix}$
Di-vacancy 3 (0, 0, 0) (0, 0, $-c$)	1.457	0·002	0·0131	$\begin{pmatrix} 0·0143 & 0·0 & 0·0 \\ 0·0 & 0·0143 & 0·0 \\ 0·0 & 0·0 & -0·4484 \end{pmatrix}$
Tri-vacancy 1 (0, 0, 0) (a, 0, 0) ($a/2$, $a\sqrt{3}/2$, 0)	1·837	0·351	0·0196	$\begin{pmatrix} 0·1225 & 0·0 & 0·0 \\ 0·0 & 0·1225 & 0·0 \\ 0·0 & 0·0 & -0·8737 \end{pmatrix}$
Tri-vacancy 2 (0, 0, 0) (a, 0, 0) ($a/2$, $-a/2\sqrt{3}$, $-c/2$)	1·838	0·351	0·0072	$\begin{pmatrix} 0·1143 & 0·0 & 0·0 \\ 0·0 & 0·1143 & 0·1621 \\ 0·0 & 0·1621 & -0·4602 \end{pmatrix}$
Tri-vacancy 3 (0, 0, 0) (a, 0, 0) (0, $a/\sqrt{3}$, $-c/2$)	1·945	0·243	0·0259	$\begin{pmatrix} -0·0348 & 0·0515 & 0·0954 \\ 0·0515 & -0·0251 & 0·0907 \\ 0·0954 & 0·0907 & -0·7715 \end{pmatrix}$

tion the distance between the split interstitials was found to be 0·481c in the case of Doneghan and Heald potential and 0·535c for the Morse potential. The relaxation field of the surrounding lattice was evaluated till 125 neighbours or shells and the magnitude of the relaxations for the first 19 shells using both potentials is shown in figure 5. The relaxations were non-radial but the magnitudes were found to be the same for atoms in each shell. A picture similar to the case of the vacancies therefore emerges since the shell labelling is the same. A striking feature of the relaxation field is that the overall nature of the relaxations for nearly all the shells is similar for both the potentials, this is in contrast to the case of vacancies (figure 4) where the two potentials gave somewhat different results. This is attributed to the strong repulsive part of the potential which plays the dominant role in determining the relaxations, the structure of the potential after the minimum modulates the relaxations. The splitting of the shells as in the case of the vacancies is also apparent. In table 5 the relaxation field of the first few shells is given where the non-radial character of the relaxation can be noted. The first shell moves outwards but the second which is in fact very close to the first one in terms of neighbour distance moves inwards. Examination of the relaxation of the higher shells shows that they all relax inwards till the sixth which again relaxes outwards. These features are common to both the potentials.

Of the three interstitial configurations, investigated using the Doneghan and Heald

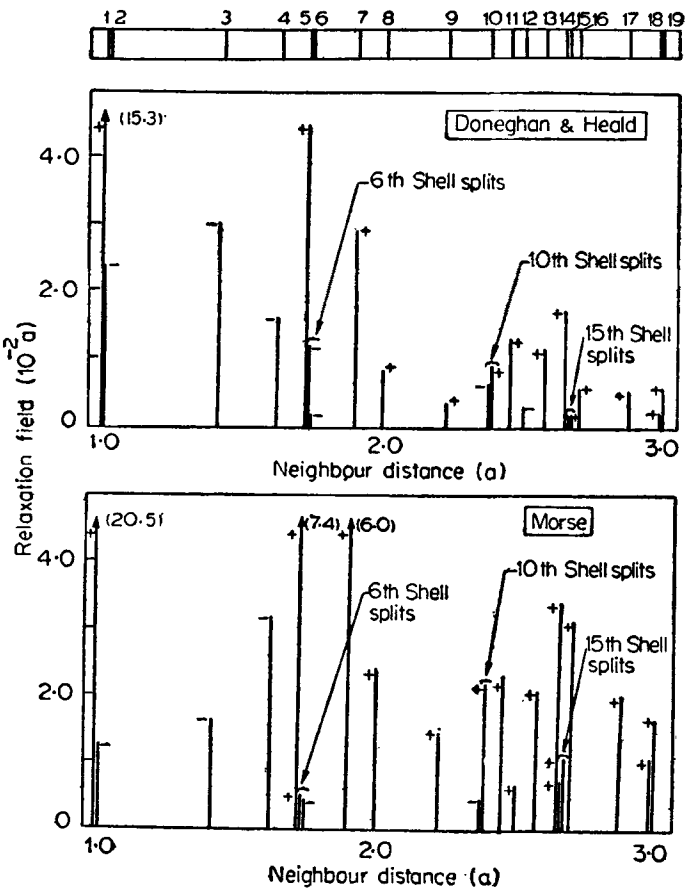

Figure 5. The relaxation field of all shells upto nineteen neighbours around a spilt interstitial. (+ and − signs indicate outward or inward relaxation).

Table 5. The relaxation field of all atoms upto ten neighbours around a split interstitial. Split interstitial (0, 0, 0).

Shell Number	Neighbour Position X	Y	Z	Relaxation field ($10^{-1}a$) D & H U_x	U_y	U_z	Relaxation field ($10^{-1}a$) Morse U_x	U_y	U_z
1	$(-a/2$	$-a/2\sqrt{3}$	$c/2)$	−1·186	−0·685	0·690	−1·561	−0·901	0·981
2	$(-a/2$	$-a\sqrt{3}/2$	$0)$	0·064	0·230	0·0	0·007	0·125	0·0
3	$(0$	$-2a/\sqrt{3}$	$c/2)$	0·0	0·293	−0·071	0·0	0·100	0·130
4	$(0$	0	$c)$	0·0	0·0	−0·158	0·0	0·0	−0·323
5	$(a$	$-2a/\sqrt{3}$	$c/2)$	0·243	−0·380	−0·018	0·370	−0·639	−0·035
6	$(3a/2$	$-a\sqrt{3}/2$	$0)$	−0·013	0·008	0·0	0·044	−0·026	0·0
	$(0$	$-a\sqrt{3}$	$0)$	0·0	0·120	0·0	0·0	0·044	0·0
7	$(a/2$	$-a\sqrt{3}/2$	$c)$	0·002	−0·244	0·148	−0·035	−0·382	04·64
8	$(-a$	$-a\sqrt{3}$	$0)$	0·001	−0·083	0·0	−0·029	−0·240	0·0
9	$(a/2$	$-7a/2\sqrt{3}$	$c/2)$	−0·030	−0·020	−0·011	−0·023	−0·141	0·022
10	$(-3a/2$	$-a\sqrt{3}/2$	$c)$	0·039	0·023	−0·048	0·035	0·020	−0·025
	$(0$	$-a\sqrt{3}$	$c)$	0·0	−0·085	−0·028	0·0	−0·212	0·058

potential the split interstitial was found to be the most stable with a formation energy of 0·86 eV. The relaxation energy was calculated to be —3·63 eV. The Morse potential, however, gave the formation energy to be 5·65 eV and a relaxation energy of —58·54 eV. These values are clearly too high but it is instructive to see why such a large magnitude is obtained. The slope of the Morse potential before the minimum is nearly two to four times larger and since this is the sensitive part of the potential and the relaxation energy depends on the square of the force an order of magnitude difference is expected. Calculations have also been done using the empirical potential of Tome *et al.* This gives a formation energy of 1·38 eV and a relaxation energy —1·47 eV. The dumb-bell length was calculated to be 0·51 c.

In table 6 the shellwise contribution to the dipole tensor using the three potentials is given. Contribution upto the 7th shell arise, because of the off centre location of the split atoms. It may be seen that the first shell contribution from the Morse potential is double that of the Doneghan and Heald potential. This is due to the larger slope of the Morse potential which also produces larger relaxations as is evident from figure 5 (compare this feature with the case of the single vacancy figure 4). The ratio P_{11}/P_{33} for the first few shells is similar but the overall contribution shows that in the case of the Doneghan and Heald potential the larger negative relaxations of the atoms of the second shell produce an overall inward contraction in the x-y plane. The Morse potential shows a similar feature but the strong outward relaxation dominates over the contraction produced by the second shell.

5.2 *Octahedral interstitial*

The octahedral interstitial was the least stable of these configurations investigated. Calculations were done using the Doneghan and Heald potential only. With the convergence factor $\alpha = 0{\cdot}75$ (see § 2) it was found that the configuration was unstable. However when α was taken as 0·05 which means that the atoms were allowed to relax in very small increments a well-defined equilibrium configuration was obtained in contrast to the remark made by Tome *et al* that this configuration migrates to more stable tetrahedral position. It may be pointed out here that the careful

Table 6. The shellwise contribution to the dipole tensor for a split interstitial.

Shell number	Atoms in shell	Doneghan and Heald $P_{11} = P_{22}$ (eV)	Doneghan and Heald P_{33} (eV)	Morse $P_{11} = P_{22}$ (eV)	Morse P_{33} (eV)	Tome *et al* $P_{11} = P_{22}$ (eV)	Tome *et al* P_{33} (eV)
1	6	3·863	8·381	8·951	16·301	3·343	8·421
2	6	—2·185	0·0	—3·187	0·0	—2·651	0·0
3	6	—2·101	—2·396	—0·767	—0·281	—2·908	—1·762
4	2	0·0	—0·231	0·0	—1·195	0·0	—2·196
5	12	—0·482	—0·136	—0·101	—0·025	—1·031	—0·280
6	6	0·431	0·0	0·015	0·0	0·0	0·0
7	12	—0·100	—0·398	—0·057	—0·221	—0·431	—1·694
Total		—0·574	5·220	4·854	14·579	—3·678	2·489

choice of the convergence factor α can only fetch a stable octahedral configuration for the interstitial, however with larger formation energy than the other possible configurations. In this configuration the relaxation energy was found to be −2·758 eV and a formation energy of 1·969 eV. The relaxation field of the first few shells is given in table 7. The first two shells relax outwards while the 3rd, 4th and 5th shells alternately relax inwards and outwards. The shellwise contribution to the dipole tensor is given in table 8. It is seen that the contribution to the dipole tensor for octahedral interstitial from the first four shells is nearly symmetric with $P_{11}=P_{22}=5{\cdot}625$ and $P_{33}=6{\cdot}447$ eV. These numbers are in good agreement with those calculated by Tome *et al* (1979) who give $P_{11}=P_{22}=5{\cdot}619$ eV and $P_{33}=6{\cdot}012$ eV using the pseudopotential and summing upto three neighbours. The contribution from the fifth shell is extremely large. This can be traced to the fifth shell lying in a region (see figure 3) where the slope of the Doneghan and Heald potential is very steep since it is artificially truncated at the fifth neighbour distance. The contribution from this shell to the dipole tensor should therefore not be taken into account.

5.3. *Tetrahedral interstitial*

Compared to the octahedral interstitial the tetrahedral interstitial was found to be more stable. However, the interstitial moved from the initial position at (0, 0, 0) which was the centroid of the irregular tetrahedron formed by the four atoms in the first and second shell to the position (0, 0, −0·021c) which corresponds to a relaxation of −0·034a along the Z-axis. The relaxation energy was found to be −8·391 eV which partly accounts for the stability of this configuration with a formation energy of 1·75 eV. The relaxation field for the first few shells is given in table 9 and the 1st, 2nd, 4th, 7th and 8th neighbours relax outward and the rest inwards. The shellwise contributions to the stress dipole tensor are given in table 8. The element $P_{11}=P_{22}=1{\cdot}770$ eV and $P_{33}=3{\cdot}319$ eV. It is important to note that a sizable contribution arises from the sixth shell because of the negative gradient of the potential. It may be noted that the pseudopotential also shows a similar slope in this region.

Table 7. The relaxation field of all atoms upto ten neighbours around an octahedral interstitial. Octahedral interstitial (0, 0, 0).

Shell number	Neighbour position X	Y	Z	Relaxation field ($10^{-1}a$) (D & H) U_x	U_y	U_z
1	(0	$a/\sqrt{3}$	$c/4$)	0·0	0·954	0·345
2	(0	$2a/\sqrt{3}$	$-c/4$)	0·0	0·036	0·026
3	($-a/2$	$a/2\sqrt{3}$	$3c/4$)	−0·015	0·009	−0·109
4	($a/2$	$5a/2\sqrt{3}$	$c/4$)	0·117	0·215	0·006
5	(0	$2a/\sqrt{3}$	$3c/4$)	0·0	0·185	0·137
6	($-a$	$2a/\sqrt{3}$	$3c/4$)	0·826	0·477	−0·345
7	(0	$a/\sqrt{3}$	$5c/4$)	0·0	−0·004	−0·024
8	($-a/2$	$7a/2\sqrt{3}$	$-c/4$)	0·003	0·040	−0·012
9	(a	$a/\sqrt{3}$	$5c/4$)	−0·006	−0·003	−0·013
10	(0	$4a/\sqrt{3}$	$c/4$)	0·0	0·044	0·002

Table 8. The shellwise contribution to the dipole tensor for octahedral and tetrahedral interstitials.

Shell number	Atoms in shell	Octahedral $P_{11} = P_{22}$ (eV)	P_{33}	Atoms in shell	Tetrahedral $P_{11} = P_{22}$ (eV)	P_{33}
1	6	5·912	5·386	1	0·0	2·260
2	6	—0·208	—0·051	3	2·448	0·300
3	6	0·130	1·141	1	0·0	0·386
4	12	—0·209	—0·029	6	—0·416	—0·346
5	6	—2·986	—6·666	3	—0·456	—0·019
6	—	—	—	6	0·437	0·827
7	—	—	—	3	—0·007	—0·084
8	—	—	—	6	—0·236	—0·005
Total 4 shells		5·625	6·447	Total 8 shells	1·770	3·319
Total 5 shells		2·639	—0·219			

Table 9. The relaxation field of all atoms upto ten neighbours around a tetrahedral interstitial. Tetrahedral interstitial (0, 0, 0).

Shell number	Neighbour position X	Y	Z	Relaxation field ($10^{-1}a$) D & H U_x	U_y	U_z
1	(0	0	$3c/8$)	0·0	0·010	1·719
2	($a/2$	$-a/2\sqrt{3}$	$-c/8$)	2·139	—1·233	—0·092
3	(0	0	$-5c/8$)	0·0	0·001	0·120
4	($-a/2$	$-a\sqrt{3}/2$	$3c/8$)	0·019	—0·031	—0·010
5	(0	$-2a/\sqrt{3}$	$-c/8$)	0·0	0·187	—0·010
6	($a/2$	$-a\sqrt{3}/2$	$-5c/8$)	0·033	—0·188	—0·079
7	($-a/2$	$-a/2\sqrt{3}$	$7c/8$)	—0·444	—0·256	0·119
8	($-a$	$-2a/\sqrt{3}$	$-c/8$)	—0·458	—0·807	—0·006
9	(0	$-2a/\sqrt{3}$	$7c/8$)	0·0	—0·005	—0·012
10	($3a/2$	$-a\sqrt{3}/2$	$3c/8$)	—0·054	0·031	—0·114

6. Conclusions

The single vacancy relaxation field shows good agreement with the results obtained earlier by Sahoo and Sahu (1978c) using the Green's function method and employing the Doneghan and Heald potential. The maximum relaxation occurs at the third neighbour shell. The dipole tensor shows a nearly isotropic behaviour with the maximum contribution from the third shell atoms. The di-vacancy configurations (*a*) and (*b*) as shown in figure 1 are found to be stable with a formation energy of 1·34 eV. Similarly the tri-vacancy configurations (*d*) and (*e*) of figure 1 are most stable with formation energy of 1·84 eV. Amongst the interstitial configurations, the *c*-axis dumb-bell is found to be most stable—a feature shared with the bcc and fcc metals. The octahedral interstitial is the least stable as has also been reported by Tome *et al* (1979). This conclusion on the dumb-bell as the stable interstitial is

in agreement with the experimental findings on hcp Zn (Ehrhart 1975). In Mg the formation energies of the split, tetrahedral and octahedral interstitial was found to be 0·86, 1·75 and 1·97 eV, respectively. The dumb-bell length was found to be 0·481c. The dipole tensor for the three interstitial configurations maintain their characteristic differences as has been discussed in the previous section.

Another important observation is that in the case of the monovacancy and split interstitial certain shells like the 6th, 10th, 15th, 20th, 28th, 31st, 32nd, 35th and 38th split into two sub-shells each. The earlier workers (Tome *et al*) do not report this observation. The introduction of a convergence factor α multiplying the relaxations in the subsequent Newton-Raphson iterations ensures a faster convergence to a stable defect configuration. A stable octahedral interstitial (however with highest formation energy among interstitials) could thus be studied even with the empirical potential of Tome *et al* who found the octahderal interstitial unstable and migrating to the tetrahedral site.

The results using the Doneghan and Heald potential compare favourably with the calculations of Tome *et al* (1979) employing the Appapillai and Heine's pseudopotential for the octahedral and tetrahedral interstitials reported by them. (They have not studied the dumb-bell interstitial). The Doneghan and Heald potential therefore is a good potential for Mg. The negative slope at the third neighbour distance as in the pseudopotential also seems to be an important requirement of the empirical potential. This view is further strengthened by the point defect studies in cubic metals made by Johnson (1973).

Acknowledgements

We gratefully wish to record our thanks to Dr D Sahoo and Dr G Venkataraman for having critically gone through the manuscript and for offering very useful suggestions.

References

Appapillai M and Heine V 1972 Tech. Rep. No. 5 SST/7/1972 (Cambridge: Cambridge Univ.)
Chang R and Falicov L M 1971 *J. Phys. Chem. Solids* **32** 465
Dagens L, Rasold M and Taylor R 1974 Tech. Rep. TP579 (Harwell: AERE)
Daou J N, Vajda P, Lucasson A and Lucasson P 1978 *Radiat. Eff.* **39** 3
Dederichs P H, Lehman C, Schober H R, Scholz A and Zeller R 1978 *J. Nucl. Mater.* **60** and **70** 176
Doneghan M and Heald P T 1975 *Phys. Status Solidi* **A30** 403
Doyama M and Cotterill R M 1967 in *Lattice defects and their interactions* ed. R R Hasiguti (New York: Gordon and Breach) p. 79
Ducharine A R and Weaver H T 1972 *Phys. Rev.* **B5** 330
Ehrhart P 1975 in *Fundamental aspects of radiation damage in metals* eds. M T Robinson and F W Young (US ERDA report conf. 751006) Vol. 1, p. 302
Eyre B L, Loretto M H and Smallman R E 1976 in *Vacancy* '76 (eds.) R E Smallman and J E Harris (The Metal Society)
Fumi F G 1955 *Philos. Mag.* **46** 1007
Harrison W A 1966 in *Psuedopotentials in the theory of metals* (New York: Benjamin)
Hohenberg P and Kohn W 1964 *Phys. Rev.* **B136** 864

Johnson R A 1973 *J. Phys.* **F3** 295
Kapoor R 1980 Pramāṇa **14** 209
Kanzaki H 1957 *J. Phys. Chem. Solids* **2** 24
Kohn W and Sham L J 1965 *Phys. Rev.* **A140** 1133
Lucasson P 1975 in *Fundamental aspects of radiation damage in metals* eds. M T Robinson and F W Young (US ERDA report conf. 751006) Vol. 1, p. 42
Manninen M, Nieminen R, Hautojarvi P 1975 *Phys. Rev.* **B12** 4012
Rasold M and Taylor R 1973 *J. Phys.* **F3** 67
Sahoo D and Sahu H K 1978a *Phys. Rev.* **B18** 6727
Sahoo D and Sahu H K 1978b *Phys. Rev.* **B18** 6738
Sahoo D and Sahu H K 1978c *Pramana* **10** 413
Sahu H K, Srinivasan S, Krishnan K 1979 *Radiat. Eff. Lett.* **50** 73
Schwartzkopff K 1969 *Acta Met.* **17** 345
Tewary V K 1973a *Adv. Phys.* **22** 757
Tewary V K 1973b *J. Phys.* **F3** 704
Tome C N, Monti A M and Savino E J 1979 *Phys. Status Solidi* **B92** 323